Lasers in Surgery and Medicine 53:141–147 (2021)

Electronic Pneumatic Injection-Assisted Dermal Drug Delivery Visualized by Ex Vivo Confocal Microscopy

Liora Bik,[1,2*] Martijn B. A. van Doorn,[2] Edyta Biskup,[1] Vinzent K. Ortner,[1] Merete Haedersdal,[1] and Uffe H. Olesen[1]

[1]*Department of Dermatology, Bispebjerg Hospital, University of Copenhagen, Bispebjerg Bakke 23, Copenhagen, 2400, Denmark*

[2]*Department of Dermatology, Erasmus MC University Medical Center Rotterdam, Doctor Molewaterplein 40, Rotterdam, 3015 GD, The Netherlands*

Background and Objectives: Electronic pneumatic injection (EPI) is a technique for dermal drug delivery, which is increasingly being used in clinical practice. However, only few studies have been reported on cutaneous drug distribution and related clinical endpoints. We aimed to visualize the immediate cutaneous drug distribution, changes in skin architecture, and related clinical endpoint of EPI.

Study Design/Materials and Methods: Acridine orange (AO) solution was administered to *ex vivo* porcine skin by EPI at pressure levels from 4 to 6 bar with a fixed injection volume of 50 µl and nozzle size of 200 µm. Immediate cutaneous distribution was visualized using ex vivo confocal microscopy (EVCM). Changes in skin architecture were visualized using both EVCM and hematoxylin and eosin-stained cryosections.

Results: The defined immediate endpoint was a clinically visible papule formation on the skin. The pressure threshold to consistently induce a papule was 4 bar, achieving delivery of AO to the deep dermis (2319 µm axial and 5944 µm lateral distribution). Increasing the pressure level to 6 bar did not lead to significant differences in axial and lateral dispersion ($P = 0.842$, $P = 0.905$; respectively). A distinctively hemispherical distribution pattern was identified. Disruption of skin architecture occurred independently of pressure level, and consisted of subepidermal clefts, dermal vacuoles, and fragmented collagen.

Conclusions: This is the first study to relate a reproducible clinical endpoint to EPI-assisted immediate drug delivery using EVCM. An EPI-induced skin papule indicates dermal drug delivery throughout all layers of the dermis, independent of pressure level settings. Lasers Surg. Med. © 2020 The Authors. *Lasers in Surgery and Medicine* published by Wiley Periodicals LLC

Key words: dermatology; skin; pneumatic device; needle-free injection; electronically-controlled; drug delivery; ex vivo confocal microscopy; device; biodistribution

INTRODUCTION

The skin functions as an effective barrier against external influences. When intending to deliver drugs intradermally, conventional syringe-needle injection is the standard of care technique to overcome this barrier. Despite their low cost, wide availability, and ease of use, needle injections have several disadvantages including pain, needle-phobia (24% of adults [1]), and the risk of needle stick injuries. To overcome these restraints, other physical delivery techniques have been developed to provide effective intradermal drug delivery [2]. These techniques include laser-assisted drug delivery, microneedling, electrochemotherapy, iontophoresis, and jet injectors [3–7].

Jet injectors are needle-free injection devices that can deliver liquids into the skin using a high-pressure stream. The recently introduced next-generation jet injectors are electronic pneumatic injection systems, which dispense fluids into the skin via accelerated, compressed gas. This minimally invasive and needle-free technique reduced occupational hazards, while providing drug delivery into the dermis leaving only a small entry point in the epidermis and a visible papule on the skin [8]. While the electronic pneumatic injection (EPI) device is more expensive and larger than spring-loaded jet injectors, clinical advantages of EPI include adjustable settings (pressure level and volume), ease of use in an outpatient clinic, minimal patient discomfort, and disposable nozzles and syringes to prevent contamination [9].

Conflict of Interest Disclosures: All authors have completed and submitted the ICMJE Form for Disclosure of Potential Conflicts of Interest and have disclosed the following: The EnerJet device was loaned to Merete Haedersdal by PerfAction as part of a research collaboration and the loan of ex vivo confocal microscopy was provided by Mavig.

*Correspondence to: Liora Bik, MD, Department of Dermatology, Bispebjerg Hospital, University of Copenhagen, Dermatology D92, Bispebjerg Bakke 23, 2400 Copenhagen, Denmark. E-mail: l.bik@erasmusmc.nl

Accepted 23 May 2020
Published online 8 June 2020 in Wiley Online Library (wileyonlinelibrary.com).
DOI 10.1002/lsm.23279

Optical imaging can be a valuable tool when the clinical utility of the various device parameters is explored. To investigate EPI parameters, skin-imitating media such as polyacrylamide gel and gelatin phantom have been used previously [10–12]. Moreover, EPI of ink followed by skin splitting and macroscopic evaluation, and histology imaging with hematoxylin and eosin (H&E) staining have also been used for optical imaging of EPI [10,11,13–15]. Although transparent media provide a clear view of injected fluid patterns, skin phantoms are currently lacking the technical refinement to mimic the biological complexity of human skin [16]. Macroscopic evaluation of skin tissue does display drug distribution but lacks detailed illustration of skin compartments and tissue alterations. Finally, cryosections can be used to inspect the cutaneous microstructure. The proneness to artifacts and inherent need for a multistep staining procedure to achieve sufficient image contrast, however, supports the use of novel optical imaging techniques to supplement traditional histology when assessing novel drug delivery techniques [17]. Fluorescence confocal microscopy can overcome these limitations by visualizing immediate EPI-induced fluorescent drug distribution without destructive tissue preparation or additional staining steps.

The ex vivo confocal microscopy (EVCM) uses a laser system to obtain high-resolution images of excised tissue [18]. The device used in the present study uses two lasers to generate both fluorescence (FCM) and reflectance confocal microscopy (RCM) images [19]. AO is most commonly used as contrast agent due to its high fluorescent yield, rapid staining and its well-established use in research [20]. EVCM is also being investigated to assess the margin control of basal cell carcinoma during micrographic Moh's surgery to shorten procedure time without sacrificing accuracy [21–28].

Visualization of immediate EPI-induced drug distribution at a microscopic level may provide a better understanding of its mechanism of action and clinical utility. Therefore, we aimed to visualize the immediate cutaneous drug distribution and changes in skin architecture using EVCM, and focus on the related clinical endpoint of EPI.

MATERIALS AND METHODS

Study Design

In this experimental *ex vivo* porcine study, immediate EPI-induced drug distribution was investigated with EVCM ($n = 22$ samples) and changes in skin architecture were investigated using EVCM and frozen histology ($n = 33$ samples). This study was conducted at the Department of Dermatology at the Bispebjerg Hospital in Copenhagen, Denmark.

Intervention

Flank skin samples from three Danish mixed-race Landrace/Yorkshire/Duroc pigs (3 months, 31–44 kg) stored at −80°C were thawed at room temperature for 30 minutes. Hair was trimmed using an electric razor. Skin samples were placed on plastic film surrounded by moist gauze for the duration of the experiment. AO (MW: 301.8 Da, excitation wavelength = 500 nm, emission wavelength = 526 nm) (Mavig, Munich, Germany) was used as a contrast agent for EVCM [29]. The stock solution of 10 mg/ml was diluted in phosphate-buffered saline to a concentration of 0.06 mg/ml. Saline was used for control injections. EPI was performed with a needle-free electronic pneumatic injection device (EnerJet2.0; PerfAction Technologies Ltd., Rehovot, Israel) (Fig. 1C). The device has a fixed nozzle size of 200 μm. A volume of 50 μl was delivered per injection (device range; 50–150 μl) with pressure levels of 4 and 6 bar corresponding 50% and 100% pressures of the device (device range; 2–6 bar). Immediately after EPI, a caliper measured the diameter of the papular skin reaction by LB. Clinical photos were captured with a DSLR camera (EOS 750D; Canon) under standardized conditions.

Biopsy Processing and Evaluation of EVCM Images

Biopsy samples were bisected at the point of injection, placed on a glass slide, and flattened using a second slide and adhesive putty. The samples were mounted on an EVCM (Vivascope 2500; Mavig) to capture images of RCM (488 nm) and FCM (785 nm), respectively, at 50% and 15% intensity. EVCM provided automatic integration of RCM and FCM into pseudo-colored composite images. Resolution of the images was 1024×1024 pixels.

Axial and lateral dispersion of AO in dermis were manually assessed by a nonblinded evaluator (LB) on FCM images. Axial distribution was defined as the perpendicular distance between the basal layer down to the deepest observed AO signal. Lateral distribution was defined as the maximum lateral expanse of AO signal, parallel to the epidermis.

Qualitative assessment of FCM, RCM, and composite images was performed by inspecting skin compartments, point of EPI entry, AO distribution pattern, and skin architecture disruption.

Evaluation of Frozen Histology

Samples for histological analyses were collected after EPI to assess changes in skin architecture. Cryosectioning, using a cryostat and freezing medium (Tissue-Tek® O.C.T.™ Compound; Sakura Finetek Europe BV, Alphen, NL), was performed to harvest vertical sections at entry point of injection and of surrounding injection site with a slice thickness of 10 μm. Sections were stained with H&E and qualitatively evaluated (LB) under a light microscope with fourfold magnification.

Statistics

Mann–Whitney *U* tests compared papule diameter and immediate drug distribution parameters from EVCM images. Data were presented as median and interquartile ranges. An α level of $P < 0.05$ was considered statistically significant. Analyses were performed in SPSS version 25 (IBM Corporation; Armonk, NY).

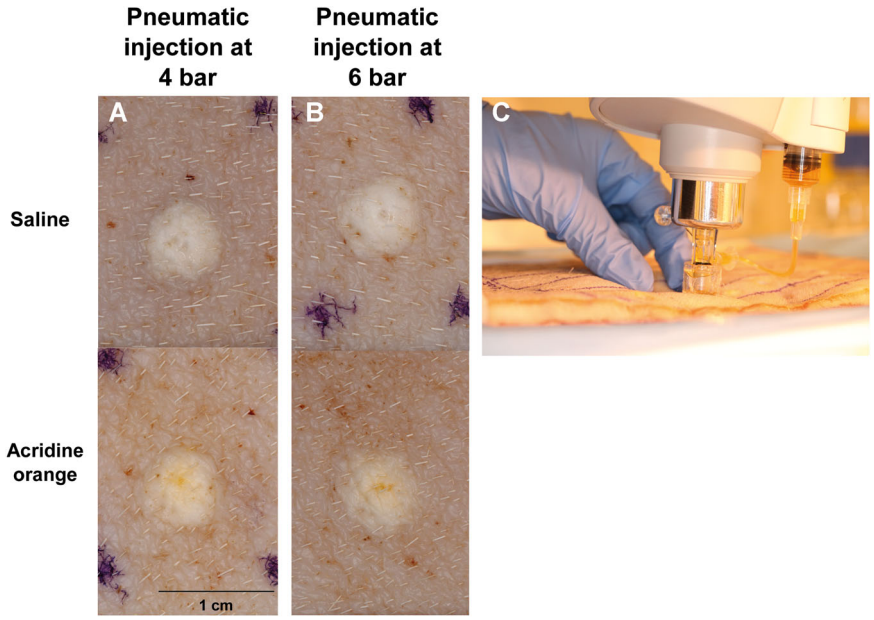

Fig. 1. Skin papule as clinical endpoint. A skin papule served as predefined, clinical endpoint after electronic pneumatic injection (50 µl/injection) at 4 bar (**A**) and 6 bar (**B**). The pressure level did not have a significant effect on papule dimensions ($P = 0.288$), with a diameter of 6.0 mm (6.0–7.0) at 4 bar and 7.0 mm at 6 bar (6.0–7.5 mm). The nozzle of the electronic pneumatic injection device is shown (**C**).

RESULTS

Papule as Clinical Endpoint

A distinct papule on the skin appeared after EPI ($n = 55$). The pressure level was titrated up to 4 bar to consistently produce a papule after each injection. The pressure level did not appear to have a significant effect on papule dimensions ($n = 33$; $P = 0.288$), with a diameter of 6.0 mm (6.0–7.0) at 4 bar and 7.0 mm at 6 bar (6.0–7.5 mm; Fig. 1A and B).

Dermal Drug Distribution

EPI with 4 and 6 bar pressure levels resulted in a comparable dispersion of contrast agent reaching upper, mid, and deep dermis with an axial distribution of 2319 µm (1500–2900 µm; 4 bar) and 2399 µm (2024–2758 µm; 6 bar; $P = 0.842$; Fig. 2; Table 1). Lateral dispersion for 4 and 6 bar pressure levels were also similar resulting in a lateral distribution of 5944 µm (5173–6861 µm; 4 bar) and 6187 µm (5351–6544 µm; 6 bar; $P = 0.905$).

The most commonly observed distribution pattern resembled a hemispherical shape for both 4 and 6 bar pressure levels (Fig. 2A-C). However, variations in shape were observed between single injections resembling, for example, triangular deep-dermal or flat upper-dermal distribution patterns (Figs. 2D-F and 3). Overall, epithelium of hair follicles and epidermal entry point of injection showed high uptake of AO. The subcutaneous layer was reached sporadically.

Skin Architecture Disruption

Confocal microscopy images demonstrated disruption of normal skin structure after EPI with multiple vacuoles surrounding the dermal injection site and sub-epidermal clefting, independent of pressure levels (Fig. 3). The epidermis was torn apart at the entry point while architectural structure of the subcutaneous layer remained intact.

Tissue disruption after EPI was confirmed on histological sections displaying vacuoles, fragmented collagen, and tissue gaps in the dermis, to a similar degree at 4 and 6 bar pressure levels (Fig. 4). Disruption was most pronounced in sections closest to the point of entry. In contrast to confocal microscopy images, signs of epidermal trauma were not visible but sporadic disruption of subcutaneous tissue was seen.

DISCUSSION

We conducted an experimental *ex vivo* porcine study in which immediate EPI-assisted drug delivery was investigated using EVCM and histological sections. Our results demonstrate that a papule on normal skin is a reproducible clinical endpoint for EPI and indicates dermal drug delivery throughout all layers of the dermis, independent of pressure level settings. In laser and light treatments, clinical endpoints already have been shown to be helpful for safe and effective treatments; for example, immediate whitening of the skin after laser treatment using Q-switched lasers for tattoo removal [30]. In our study, we found that a skin papule has been consistently produced with a minimum pressure level of 4 bar. However, this

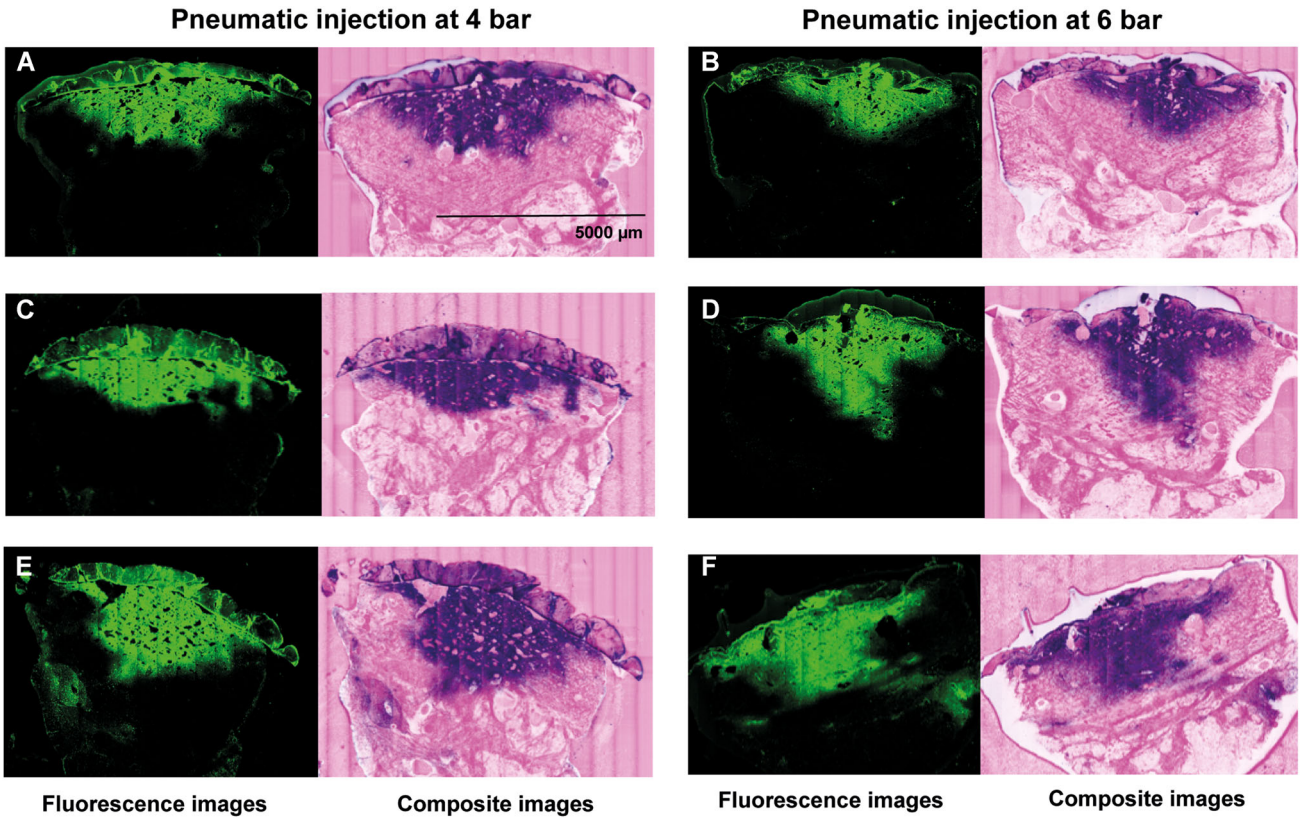

Fig. 2. Electronic pneumatic injection induces deep dermal drug delivery. Fluorescence and composite images were captured using an ex vivo confocal microscope. Images show comparable fluorescent drug distribution of acridine orange in deep dermis following electronic pneumatic injection at 4 and 6 bar pressure level (acridine orange solution is green on fluorescence images and purple on composite images). The most commonly observed distribution pattern was hemispherical (**A**, **B**, and **C**). Mild variations in shape have been observed for both pressure levels (**D**, **E**, and **F**). (**A**–**F**) display separate representative biopsies.

pressure level may not be directly translated into a clinical setting, as human dermis is generally thinner than porcine skin. Also, the pressure level required to induce a papule may vary when treating different anatomical locations or skin lesions with higher consistencies (e.g., hypertrophic scars or keloids).

In this study, we used EVCM as a high-resolution imaging technique. The EVCM had an acquisition time of approximately 3–5 minutes, while preparation of cryosections requires 20–45 minutes per tissue sample [22]. Beside the benefit of minimal waiting time, tissue integrity remained intact and provided a realistic view on skin architecture and immediate drug distribution. Analyses of EVCM images showed that both 4 and 6 bar pressure levels generated deep dermal drug delivery. Spatial distribution of dermal drug delivery has also been investigated using a similar EPI device at 3.1, 3.9, and 4.6 bar pressure levels and 80 µl injection volume by Erlendsson et al. [31], however, with ink as a contrast agent and assessment of drug distribution on histological sections only. In the study by Erlendsson et al., lateral dispersion was found to be pressure independent for individual injections, which is similar to our results. Notably, the lateral dispersion increased when stacking two consecutive injections at the same site, however, stacking of injections was not investigated in our study. For axial dispersion, a significant increase was observed when the highest pressure level of 4.6 bar was used for individual injections. This suggests that axial dispersion could be pressure dependent at lower pressure levels, while the dispersion is pressure independent between

TABLE 1. Spatial Distribution of Acridine Orange

Pressure level	Number of biopsies	Axial, median in µm (IQR)	Lateral, median in µm (IQR)
4 bar	10	2319 (1500–2900)	5944 (5173–6861)
6 bar	9	2399 (2024–2758)	6187 (5351–6544)

Spatial distribution of acridine orange in porcine dermis administered with electronic pneumatic injection, visualized by ex vivo confocal microscopy, defined as axial and lateral dermal drug distribution.
IQR, interquartile range.

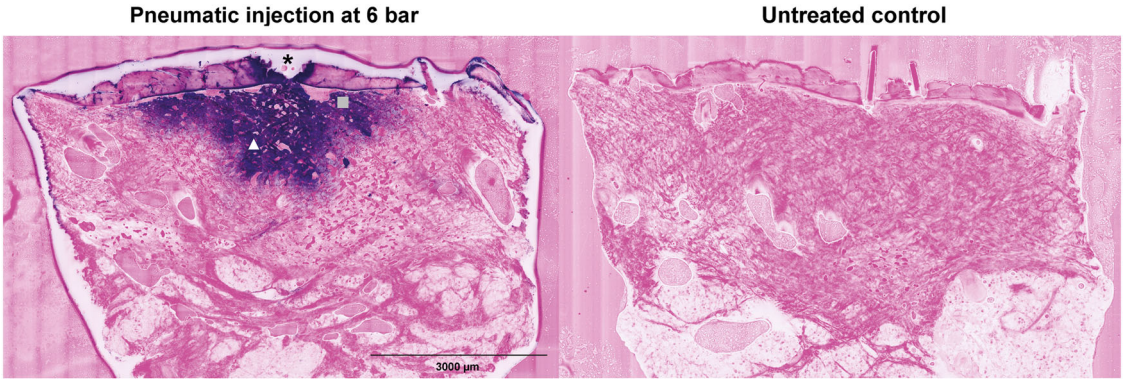

Fig. 3. Disrupted skin architecture by electronic pneumatic injection. Composite image showing skin architecture (pink) disrupted by electronic pneumatic injection with acridine orange (purple) at 6 bar pressure level (left) and an untreated biopsy (right) using ex vivo confocal microscopy. Tissue disruption was similar for 4 and 6 bar pressure level. *, epidermal trauma at entry point of injection; ■, clefting between stratum basale and dermis; ▲, vacuoles in the dermis.

4 and 6 bar according to our findings. Seok et al. [13] has found similar EPI-induced spatial distribution for 6 bar with an axial distribution of 2323 µm compared with 2399 µm found in this study. Although no difference in spatial distribution was observed between 4 and 6 bar pressure level, we did observe a variation in distribution patterns, including hemispherical dispersion projecting from injection site, a deep-dermal distribution with a triangular appearance, and a flat upper-dermal distribution with a small penetration depth. This variation could possibly be explained by a difference in tissue consistencies within the skin sample and/or variation in

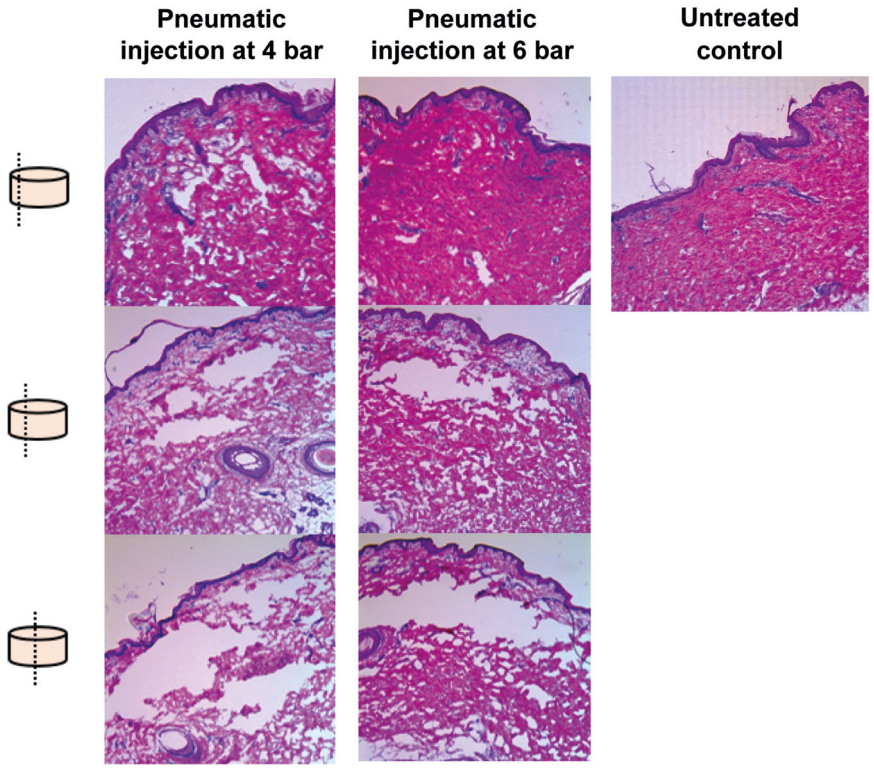

Fig. 4. Skin architecture disruption visualized on histology images. On frozen tissue sections, skin architecture disruption induced by electronic pneumatic injection was observed as vacuoles, fragmented collagen, and tissue gaps in the dermis. Three sections are shown of one representative biopsy for both 4 and 6 bar. The tissue disruptions are more prominent in close proximity to the point of entry. Untreated control with intact skin architecture is shown for comparison.

residue formation on top of the skin. Michinaka et al. [32] showed that the dispersion area of spring-driven jet injector relates inversely to the size of injected particles but proportionally to injection volume. Rohilla et al. [33] showed a significant effect on penetration depth, which could alter the distribution pattern, when comparing fluid viscosity *in vitro* using a spring-driven jet injector. The different working mechanisms of spring-driven jet injectors and EPI, however, preclude direct comparison of device parameters.

EPI-induced dermal skin structure disruption was visualized by EVCM images and histological sections, although with a slightly different presentation. The distinction could be explained by tissue alterations due to slow freezing, biopsy storage at −80℃, and tissue processing, which may have stretched the fragile tissue, exposing fragmented collagen and tissue gaps on histological sections [17]. Skin structure disruption of the dermis plays an important role in long-term effects of treatments focusing on skin remodeling. It activates the wound-healing process including the remodeling phase, which consists of collagen augmentation, crosslinking, and skin contraction for at least 6 months [12,15,34]. Previous studies have related EPI-induced neocollagenesis to a beneficial long-term effect of 4–6 months in rhytids [12,35], in contrast to the short-term effects seen after needle injection with, for example, hyaluronic acid and saline [35].

EPI's ability to provide deep dermal drug delivery may be particularly advantageous for dermatological conditions in which treatment specifically targets the dermis. In accordance, preliminary positive outcomes have been reported for keloids, acne scars, wrinkle treatment, palmar and axillar hyperhidrosis, local anesthetics, photo dynamic therapy for non-melanoma skin cancer, and nail psoriasis [36–41]. However, none of these studies focused on a clinical endpoint as in our study, which is important for guiding the treating physician in clinical practice.

Limitations in visualization of EPI-induced dermal drug delivery in this study includes the use of *ex vivo* pig skin to model *in vivo* human skin [42], uncertainty to what degree drugs used in clinical practice will behave similarly to AO, the lack of kinetic evaluation of cutaneous drug distribution, and the lacking assessment of a minimum threshold for AO detection with EVCM. Moreover, cryosectioning was used to assess tissue morphology with a moderate risk of artifacts, image assessment lacked a blinded second evaluator, and in order to standardize interventions, we only applied a fixed volume of 50 μl compared at 4 and 6 bar.

For future research we suggest to further investigate other factors that could impact the spatial dispersion of EPI, including different injection volumes, variation in residue formation on top of the skin, and stacking of injections.

CONCLUSION

This is the first study that relates a reproducible clinical endpoint to immediate EPI-assisted drug delivery and tissue disruption using reflectance and fluorescence confocal microscopy images and histological sections. An EPI-induced skin papule indicates dermal drug delivery throughout all layers of the dermis, independent of pressure level settings.

ACKNOWLEDGMENTS

The authors would like to thank Diana Høeg for her contribution in obtaining the EVCM images.

REFERENCES

1. Taddio A, Ipp M, Thivakaran S, et al. Survey of the prevalence of immunization non-compliance due to needle fears in children and adults. Vaccine 2012;30(32):4807–4812.
2. Haedersdal M, Erlendsson AM, Paasch U, Anderson RR. Translational medicine in the field of ablative fractional laser (AFXL)-assisted drug delivery: A critical review from basics to current clinical status. J Am Acad Dermatol 2016;74(5): 981–1004.
3. Waghule T, Singhvi G, Dubey SK, et al. Microneedles: A smart approach and increasing potential for transdermal drug delivery system. Biomed Pharmacother 2019;109: 1249–1258.
4. Hogan NC, Taberner AJ, Jones LA, Hunter IW. Needle-free delivery of macromolecules through the skin using controllable jet injectors. Expert Opin Drug Deliv 2015;12(10): 1637–1648.
5. Wenande E, Anderson RR, Haedersdal M. Fundamentals of fractional laser-assisted drug delivery: An in-depth guide to experimental methodology and data interpretation. Adv Drug Deliv Rev 2019;S0169–409X(19)30185–1.
6. Ita K. Transdermal iontophoretic drug delivery: Advances and challenges. J Drug Target 2016;24(5):386–391.
7. Seyed Jafari SM, Jabbary Lak F, Gazdhar A, Shafighi M, Borradori L, Hunger RE. Application of electrochemotherapy in the management of primary and metastatic cutaneous malignant tumours: A systematic review and meta-analysis. Eur J Dermatol 2018;28(3):287–313.
8. Kobus KF, Dydymski T. Quantitative dermal measurements following treatment with AirGent. Aesthet Surg J 2010;30(5): 725–729.
9. Barolet D, Benohanian A. Current trends in needle-free jet injection: An update. Clin Cosmet Investig Dermatol 2018; 11:231–238.
10. Schramm-Baxter J, Mitragotri S. Needle-free jet injections: Dependence of jet penetration and dispersion in the skin on jet power. J Control Release 2004;97(3):527–535.
11. Schoubben A, Cavicchi A, Barberini L, et al. Dynamic behavior of a spring-powered micronozzle needle-free injector. Int J Pharm 2015;491(1–2):91–98.
12. Cho SB, Kwon TR, Yoo KH, Oh CT, Choi EJ, Kim BJ. Transcutaneous pneumatic injection of glucose solution: A morphometric evaluation of in vivo micropig skin and tissue-mimicking phantom. Skin Res Technol 2017;23(1):88–96.
13. Seok J, Oh CT, Kwon HJ, et al. Investigating skin penetration depth and shape following needle-free injection at different pressures: A cadaveric study. Lasers Surg Med 2016;48(6):624–628.
14. Simmons JA, Davis J, Thomas J, et al. Characterization of skin blebs from intradermal jet injection: Ex-vivo studies. J Control Release 2019;307:200–210.
15. Chun SH, Kim BY, Natari S, Kim IH. Needle-free pneumatic injection device; histologic assessment using a rat model and parameter comparison in predicting collagen synthesis degree. Lasers Surg Med 2019;51(3):278–285.
16. Dąbrowska AK, Rotaru GM, Derler S, et al. Materials used to simulate physical properties of human skin. Skin Res Technol 2016;22(1):3–14.
17. Taqi SA, Sami SA, Sami LB, Zaki SA. A review of artifacts in histopathology. J Oral Maxillofac Pathol 2018;22(2):279.

18. Longo C, Ragazzi M, Rajadhyaksha M, et al. In vivo and ex vivo confocal microscopy for dermatologic and Mohs surgeons. Dermatol Clin 2016;34(4):497–504.
19. Cinotti E, Perrot JL, Labeille B, Cambazard F, Rubegni P. Ex vivo confocal microscopy: An emerging technique in dermatology. Dermatol Pract Concept 2018;8(2):109–119.
20. Gadjiko M, Rossi AM. Ex vivo confocal microscopy: A diagnostic tool for skin malignancies. Cutis 2017;100(2):81–83.
21. Karen JK, Gareau DS, Dusza SW, Tudisco M, Rajadhyaksha M, Nehal KS. Detection of basal cell carcinomas in Mohs excisions with fluorescence confocal mosaicing microscopy. Br J Dermatol 2009;160(6):1242–1250.
22. Longo C, Pampena R, Bombonato C, et al. Diagnostic accuracy of ex vivo fluorescence confocal microscopy in Mohs surgery of basal cell carcinomas: A prospective study on 753 margins. Br J Dermatol 2019;180(6):1473–1480.
23. Pérez-Anker J, Ribero S, Yélamos O, et al. Basal cell carcinoma characterization using fusion ex vivo confocal microscopy: A promising change in conventional skin histopathology. Br J Dermatol 2019;182:468–476.
24. Longo C, Rajadhyaksha M, Ragazzi M, et al. Evaluating ex vivo fluorescence confocal microscopy images of basal cell carcinomas in Mohs excised tissue. Br J Dermatol 2014; 171(3):561–570.
25. Flores ES, Cordova M, Kose K, et al. Intraoperative imaging during Mohs surgery with reflectance confocal microscopy: Initial clinical experience. J Biomed Opt 2015;20(6):61103.
26. Gareau DS, Li Y, Huang B, Eastman Z, Nehal KS, Rajadhyaksha M. Confocal mosaicing microscopy in Mohs skin excisions: Feasibility of rapid surgical pathology. J Biomed Opt 2008;13(5):054001.
27. Patel YG, Nehal KS, Aranda I, Li Y, Halpern AC, Rajadhyaksha M. Confocal reflectance mosaicing of basal cell carcinomas in Mohs surgical skin excisions. J Biomed Opt 2007;12(3):034027.
28. Bennassar A, Vilata A, Puig S, Malvehy J. Ex vivo fluorescence confocal microscopy for fast evaluation of tumour margins during Mohs surgery. Br J Dermatol 2014;170(2): 360–365.
29. Byvaltsev VA, Bardonova LA, Onaka NR, et al. Acridine orange: A review of novel applications for surgical cancer imaging and therapy. Front Oncol. 2019;9:925.
30. Wanner M, Sakamoto FH, Avram MM, et al. Immediate skin responses to laser and light treatments: Therapeutic endpoints: How to obtain efficacy. J Am Acad Dermatol 2016;74(5):821–833.
31. Erlendsson AM, Haedersdal M, Rossi AM. Needle-free injection assisted drug delivery-histological characterization of cutaneous deposition. Lasers Surg Med 2019; 52:33–37.
32. Michinaka Y, Mitragotri S. Delivery of polymeric particles into skin using needle-free liquid jet injectors. J Control Release 2011;153(3):249–254.
33. Rohilla P, Marston JO. In-vitro studies of jet injections. Int J Pharm 2019;568:118503.
34. Rolin G, Binda D, Tissot M, et al. In vitro study of the impact of mechanical tension on the dermal fibroblast phenotype in the context of skin wound healing. J Biomech 2014;47(14): 3555–3561.
35. Levenberg A, Halachmi S, Arad-Cohen A, Ad-El D, Cassuto D, Lapidoth M. Clinical results of skin remodeling using a novel pneumatic technology. Int J Dermatol 2010;49(12): 1432–1439.
36. Kim HK, Park MK, Kim BJ, Kim MN, Kim CW, Kim SE. The treatment of keloids with pneumatic technology: A pilot study. Int J Dermatol 2012;51(12):1502–1507.
37. Lee JW, Kim BJ, Kim MN, Lee CK. Treatment of acne scars using subdermal minimal surgery technology. Dermatol Surg 2010;36(8):1281–1287.
38. Han TY, Lee JW, Lee JHK, et al. Subdermal minimal surgery with hyaluronic acid as an effective treatment for neck wrinkles. Dermatol Surg 2011;37(9):1291–1296.
39. Vadeboncoeur S, Richer V, Nantel-Battista M, Benohanian A. Treatment of palmar hyperhidrosis with needle injection versus low-pressure needle-free jet injection of onabotulinumtoxina: An open-label prospective study. Dermatol Surg 2017;43(2):264–269.
40. Gong Y, Labh S, Jin Y, et al. Needle-free injection of 5-aminolevulinic acid in photodynamic therapy for the treatment of non-melanoma skin cancer. Dermatol Ther 2016;29(4):255–262.
41. Nantel-Battista M, Richer V, Marcil I, Benohanian A. Treatment of nail psoriasis with intralesional triamcinolone acetonide using a needle-free jet injector: A prospective trial. J Cutan Med Surg 2014;18(1):38–42.
42. Schramm J, Mitragotri S. Transdermal drug delivery by jet injectors: Energetics of jet formation and penetration. Pharm Res 2002;19(11):1673–1679.